

# Near-infrared imaging polarimetry of dusty young stars

A. S. Hales<sup>1</sup>, T. M. Gledhill<sup>2</sup>, M. J. Barlow<sup>1</sup> and K.T.E. Lowe<sup>2</sup>

<sup>1</sup>Department of Physics and Astronomy, University College London, Gower Street, London WC1E 6BT

<sup>2</sup>School of Physics, Astronomy and Mathematics, University of Hertfordshire, College Lane, Hatfield, AL10 9AB

21 July 2021

## ABSTRACT

We have carried out JHK polarimetric observations of eleven dusty young stars, by using the polarimeter module IRPOL2 with the near-IR camera UIST on the 3.8-m United Kingdom Infrared Telescope (UKIRT). Our sample targeted systems for which UKIRT-resolvable discs had been predicted by model fits to their spectral energy distributions. Our observations have confirmed the presence of extended polarized emission around TW Hya and around HD 169142. HD 150193 and HD 142666 show the largest polarization values among our sample, but no extended structure was resolved. By combining our observations with HST coronographic data from the literature, we derive the J- and H-band intrinsic polarization radial dependences of TW Hya's disc. We find the disc's polarizing efficiency is higher at H than at J, and we confirm that the J- and H-band percentage polarizations are reasonably constant with radius in the region between 0.9 and 1.3 arcseconds from the star. We find that the objects for which we have detected extended polarizations are those for which previous modelling has suggested the presence of flared discs, which are predicted to be brighter than flat discs and thus would be easier to detect polarimetrically.

**Key words:** stars : evolution – Circumstellar matter – planetary systems: protoplanetary discs – infrared : stars – techniques: polarimetric

## 1 INTRODUCTION

The discovery of the Vega-phenomenon in 1984 is considered one of the most important achievements of the IRAS space telescope. It discovered that several main sequence (MS) stars, including Vega, exhibited large mid- and far-infrared excesses that could not be ascribed to pure photospheric emission (Aumann et al. 1984). Such excesses were attributed to a disc or ring of solid particles surrounding the stars, later termed 'debris-discs', and great interest was taken in these objects because of their relevance to the formation of planetary systems.

The case of young low- and intermediate-mass systems, such as T Tauri and Herbig Ae/Be (HAeBe) stars, is of particular interest (Yudin, 2000; Waters & Waelkens, 1998). These stars are considered to be precursors of classic Vega-like stars, such as  $\beta$  Pictoris,  $\epsilon$  Eridani, HR 4796A, Fomalhaut and Vega itself. While planetary bodies are thought to have already formed in Vega-like systems (Aumann et al. 1984; Beust et al., 1996; Natta et al., 2004), the circumstellar environments of T Tauri and HAeBe stars probably represent an early phase of planet formation (Bouwman et al., 2001).

From high resolution optical spectra of a sample of young dusty stars, the majority in common with our cur-

rent sample and classified as HAeBe or T Tauri stars on the basis of their emission line spectra, Dunkin, Barlow & Ryan (1997a; 1997b) found that analysis of their absorption line spectra yielded surface gravities typical of MS stars, suggesting that they had already arrived on the MS. These type of objects have been referred to as 'transition' objects (Malfait, Bogaert & Waelkens, 1998) or 'dusty' Vega-excess stars (Dent, Greaves & Coulson, 2005) and they are nowadays thought to play a pivotal role in our understanding on the transition between the pre-MS (T Tauri and HAeBe stars) and the MS (Vega-like stars).

Many issues remain unclear regarding the circumstellar structures of these 'transition' objects, in particular, whether they are surrounded by flat discs or spherical envelopes is still not determined (Vink et al., 2002). Based on their spectral energy distributions, Meeus et al. (2001) introduced a classification of HAeBe stars into two groups: Group I objects have an almost flat or even rising 20–100  $\mu\text{m}$  spectral energy distribution (SED), which can be well modelled by a flaring disc (Dullemond & Dominik, 2004). On the other hand, Group II objects have a much bluer IR SED, and are believed to be associated with self-shadowed non-flared discs, which are predicted to be smaller in spatial extent than those of Group I sources.

High-contrast, high-spatial resolution, imaging close to

bright central stars is required to test the validity of these models. Despite the efforts of many groups, limitations on instrumental capabilities have to date kept the number of directly imaged discs to a very low-number (see Zuckerman (2001) for a review). When only SEDs are available, not all parameters can be uniquely determined, e.g. the grain-size distribution and the spatial density profile are usually not separable.

Imaging polarimetry provides a powerful technique for detecting dust-discs around bright stars. Since only the light from the discs is expected to be polarized, the bright central stars are automatically suppressed in polarized light images. The utility of imaging polarimetry was demonstrated over ten years ago when Gledhill, Scarrott & Wolstencroft (1991) detected polarized emission from the nearby Beta Pictoris disc ( $> 1000$  AU in radius at a distance of 19.3 pc; Crifo et al. (1997)). The light was found to be 17% polarized and extended up to 30 arcseconds from the star (R-waveband). Kuhn, Potter & Parise (2001) also used imaging polarimetry to detect polarized light around the A5Ve star HD 169142. More recently, using the Very Large Telescope (VLT), Apai et al. (2004) tested the power of imaging polarimetry on an 8-m class telescope, detecting the presence of polarized emission as close as 0.1 arcsecond ( $\sim 6$  AU) from the classical T Tauri star TW Hya.

We have carried out a JHK imaging polarimetry survey for a sample of ten ‘transition’ objects (so called ‘dusty’ Vega-excess stars), selected from the surveys of Sylvester et al. (1996) and Mannings & Barlow (1998), along with TW Hya. Modelling of their SEDs had predicted angular sizes that could be resolvable at near-infrared (near-IR) wavelengths using the near-IR imaging instrument UIST on the 3.8-m United Kingdom Infrared Telescope (Sylvester & Skinner, 1996; Sylvester, Skinner & Barlow, 1997). Our primary aim is to detect the signature of extended polarized emission from a scattering disc around the target stars. Note that even if the disc is too small to be resolved with UKIRT, a net polarization can be observed, indicating the presence and orientation of a disc on the sky.

Section 1.1 describes our target sample and basic selection criteria. §2 reports on the observations and §3 on the data reduction; Results are presented in §4, and discussed in §5.

### 1.1 Target sample

We have selected a sample of ten young stars with dust discs from the surveys of Sylvester et al. (1996) and Mannings & Barlow (1998). All targets show mid- and far-IR excesses due to warm and cold dust grains. Most of them have been thoroughly studied using spectrophotometric techniques. Spectral types, effective temperatures, surface gravities, elemental abundances and overall line-emission characteristics are available for the majority of the sample (Dunkin, Barlow & Ryan, 1997a; Dunkin, Barlow & Ryan, 1997b). A summary of our sample is shown in Table 1, where we have listed respectively their names, spectral classification, infrared excess fractions  $L_{\text{IR}}/L_{\star}$ , distances and V-band magnitudes (as listed in the SIMBAD database).

The IR excesses of our targets are all much larger than those of true Vega-like stars (which are typically  $L_{\text{IR}}/L_{\star} < 10^{-3}$  for Vega-like stars; Sylvester et al. (1996)).

Their surface gravities indicate they have recently reached the MS (Dunkin, Barlow & Ryan, 1997a; Dunkin, Barlow & Ryan, 1997b). HD 123160, HD 123356, HD 141569 and HD 145263 have relatively low IR excesses compared to the rest of our sample. The remaining stars have considerably larger IR excesses ( $L_{\text{IR}}/L_{\star} > 0.1$ ), suggesting that they might be in a somewhat younger evolutionary state. HD 142666, HD 143006, HD 144432 and HD 169142 have near-IR excesses attributable to hot dust emission, resulting in (J-H) and (H-K) colours coincident with the locus of HAeBe and T Tauri stars (Sylvester et al., 1996). It has been proposed that the dust responsible for the near-IR excesses is a main agent for the optical polarization, and thus that Vega-like ‘prototypes’ showing almost no near-IR excess should present low polarization values (Yudin, 2000). HD 142666, HD 143006, HD 144432 and HD 169142 have been detected in CO in the survey by Dent et al. (2005), indicating they still have substantial gas content.

## 2 OBSERVATIONS

The J-band data presented in this work was acquired on April 29th 2003, using the dual-beam polarimeter module IRPOL2 in conjunction with the near-IR camera UIST on UKIRT at Mauna Kea observatory. The resulting field of view was of  $15 \times 60$  arcseconds, with 0.12 arcseconds per pixel. H- and K-band data for TW Hya, HD 150193 and HD 141569 were also acquired, on April 30th 2003, using the same observing procedure.

Dual-beam imaging polarimetry was obtained using a lithium niobate Wollaston prism, along with a rotating half-wave plate. By observing at four different half-wave plate positions (separated by 22.5 degrees), linear polarimetry is acquired. A detailed description of this standard dual-beam polarimetry configuration can be found in Berry & Gledhill (2003). Basically, two orthogonally polarized images are simultaneously recorded. The subtraction of these two images leads to the suppression of unpolarized light (mainly from the central star), and to the highlighting of polarized light (e.g. scattered light from the disc).

We observed a total of 11 objects. Since most of our targets are bright ( $K < 8$ ), several short exposures ( $< 1$  s) were co-added, in order to overcome saturation problems. Typical integration times ranged from 315 to 475 seconds. A non-destructive readout mode was used (ND+STARE). Point Spread Function (PSF) and flux calibrators were regularly interspersed, and polarized standards from the UKIRT calibration catalogue were also observed. In order to minimise the effects of pixel to pixel variations in the detector on derived polarization values, each measurement was repeated at 3 different array (jitter) positions.

## 3 DATA REDUCTION

All data were identically reduced using the STARLINK data-reduction pipeline ORAC-DR<sup>\*</sup>. Dark subtraction and flat-fielding are carried out, and the dual-beam imaging polarimetry package POLPACK (Berry & Gledhill, 2003) was

\* <http://www.oracdr.org/>

then used to perform component image alignment and to combine the data to form resultant I, Q and U Stokes images. Propagation of the variance estimates from the raw data through the calculation provides errors on the final I, Q and U images, and on the derived polarized quantities P and PI (degree of polarization and polarized flux, respectively).

The values of P presented in this work correspond to the degree of polarization averaged over 0.36 arcsecond square bins ( $3 \times 3$  pixels), after applying a  $2\sigma$  cut. In this way, only measurements with an error in the degree of polarization of less than one-half of the polarization are considered.

## 4 RESULTS

### 4.1 J- band imaging polarimetry and photometry

J- band photometry is presented in Table 2, together with 2MASS photometry. The photometric values derived from our measurements are generally in good agreement with the 2MASS values. HD 143006's J- band magnitude shows a 0.23 magnitude deviation with respect to previous J- band photometry, suggesting that the object has brightened since the 2MASS measurements. HD 169142's J- band magnitude is also fainter than the 2MASS photometry, but is consistent with J- band measurements from Sylvester et al. (1996).

Table 3 presents measured integrated polarizations for our targeted stars. In the case of resolved centrosymmetric patterns (as in the cases of TW Hya and HD 169142), the integrated polarization will appear less than the actual resolved polarizations, since integrating the polarization vectors over all orientations can average to zero. As an example, TW Hya's maximum resolved polarization is  $15 \pm 0.5\%$  at 1.6 arcseconds from the star, while its integrated polarization is  $0.233 \pm 0.025\%$ . The J- band instrumental polarization was estimated from observations of unpolarized standards, which showed percentage polarization levels of less than 0.5 percent. These values represent the real precision of our polarimetric measurements (mostly residuals from the alignment procedure), and should again not be confused with the statistical errors on the integrated polarizations quoted in Table 3.

Targets for which we detect evidence of polarizing circumstellar material are discussed individually below (TW Hya, HD 169142, HD 150193 and HD 142666). The remaining stars from our sample do not show any evidence of dusty polarizing discs. This suggests that their polarization levels are too faint to be detected by our observations, as exemplified by the non-detection of the disc around HD 141569. The intensity distribution of HD 141569's ring-like disc is known to peak at 3.3 arcseconds from the star (Augereau et al., 1999), a scale resolvable with UKIRT. However our J-band polarimetric observations were not able to detect it. Combining the HST J-band coronographic observations of HD 141569's disc (Augereau et al., 1999) and our polarimetric data, we derive upper-limits on the polarization level of HD 141569's disc. From this we conclude the disc is so faint that even if it was 100% polarized it would still fall below our detection limit. Augereau et al.'s (1999) HST observations showed that the surface brightness of HD 141569's disc

peaks at  $0.199 \pm 1.2$  mJy arcsec $^{-2}$ . This is one order of magnitude fainter than that of TW Hya's disc ( $5.7 \pm 1.4$  mJy arcsec $^{-2}$ ; Weinberger et al. (2002)), and could explain why the disc around TW Hya could be seen in polarized light, while the one around HD 141569 was not.

J-band imaging polarimetry of four of our eleven targets is presented in Figures 1, 2, 4 and 5 using the same format for each target. Polarization vector maps are superimposed upon total intensity contours. Total intensity grey-scales are also plotted, with the purpose of highlighting the position of the central source. The polarization vectors are oriented parallel to the E vector, with their length proportional to the degree of linear polarization, as indicated by the scale vector on each diagram.

### TW Hya:

Our observations show a centro-symmetric polarization pattern (Figure 1, left panel), revealing the signature of a scattering disc seen near to face-on. The polarization values increase with increasing radius, up to  $\sim 15\%$  at 1.6 arcseconds, although these have larger uncertainties than those close in. We note the  $\sim 15\%$  percentage polarization values we measure at 1.6 arcseconds include direct unpolarized flux from the star in the estimate of the disc's total scattered light intensity, and so represent a lower limit on the disc's intrinsic polarization. Please refer to Section 5 and Figure 9, left panel, for an estimate on the intrinsic polarization of TW Hya's disc. We estimate the extension of the polarizing disc by comparing the polarized intensity (PI) radial profile of TW Hya to the total intensity radial profile of the PSF reference star HIP54690 (Figure 1, right panel). Extended polarized structure can be traced from  $\sim 0.4$  arcseconds up to at least  $\sim 1.5$  arcseconds. This is comparable to the extension of TW Hya's polarizing disc as seen in the Ks- band with the VLT (1.4 arcseconds in radius, Apai et al. (2004)).

### HD 169142:

Our UKIRT observations just marginally resolve a centro-symmetric pattern around HD 169142 (Figure 2, left panel). The PI radial profile of HD 169142 (Figure 2, right panel) shows the detection of an extended polarizing disc from  $\sim 0.4$  to about 1.2 arcseconds radius. Inspection of the Q-polarization image of HD 169142 (Figure 3, left panel) reveals a clear modulation with angle around the star (Figure 3, right panel). The modulation reveals the presence of an extended distribution of dust, as has already been shown by Kuhn et al. (2001).

### HD 150193:

Recent adaptive optics H-band coronographic observations of the binary system HD 150193 A-B (1.1 arcseconds separation) at the 8.2-m Subaru telescope (Fukagawa et al., 2003) have revealed the presence of a scattering disc around the primary star, extending from the edge of the coronographic mask (0.5 arcseconds radius, or 50 AU) to about 1.3 arcseconds. An asymmetry of the disc in the direction of the binary companion was detected, suggesting that the companion has

a distorting effect on the disc structure. HD 150193 A is known to be a A2 IV Herbig Ae star (Mora et al., 2001), whilst HD 150193 B has recently been classified as a classical T Tauri star (Bouvier & Corporon, 2001).

Our J-band observations show polarization vectors aligned at a position angle (PA) of approximately 57 degrees, measured from North to East (Figure 4, left panel). This sort of pattern is usually associated with scattering in an unresolved geometry. In fact, the J-band PI radial profile of HD 150193 A shows no extension when compared to the total intensity radial profile of the PSF reference star (Figure 4, right panel).

HD 150193 presents the highest integrated percentage polarization of the sample (3.15% at PA=57 degrees), of which a significant part is thought to be interstellar in nature (HD 150193 is located near the edge of the  $\rho$  Ophiuchus cloud). Yudin (2000) estimated the interstellar polarization to be 2.5 % at 21 degrees PA in the V- band, and concluded that the intrinsic optical polarization of HD 150193 is 4.2%, at 65 degrees PA. By comparing our measured PA and Yudin's intrinsic PA, we conclude that most of the polarization we detect in the J band must be intrinsic to the disc, with a large amount of polarizing material in the line of sight of the star. We note that the integrated polarization that we measure around the system of 3.15% is in agreement with Whittet et al. (1992), given systematic errors of 0.1 – 0.2%.

#### HD 142666:

This A8Ve star (Dunkin, Barlow & Ryan, 1997b) was catalogued as a probable Herbig Ae star by Gregorio-Hetem et al. (1992), yet no CS disc has been directly observed around it. HD 142666 shows evidence of CS activity; a double-peaked  $H\alpha$  profile (Dunkin, Barlow & Ryan, 1997b), photometric variability, and a large IR excess attributed to CS dust (Sylvester et al., 1996). Meeus, Waelkens & Malfait (1998) interpreted the variable photometric behaviour of HD 142666 as evidence of clumps of CS material crossing the line of sight of the star. If the CS structure is flattened, then the CS disc would be more likely to be orientated edge-on. Yudin, Clarke and Smith (1999) measured 0.5% intrinsic optical polarization, considerably larger than those of the Vega-like 'prototypes' (0.02% and 0.007% for  $\beta$  Pictoris and Vega respectively; Leroy (1993)).

Figure 5, left panel, shows our J-band imaging polarimetry of HD 142666. HD 142666 presents a polarization pattern with vectors aligned at  $\sim 75$  degrees PA and a 1.2 % mean polarization. As with HD 150193, the PI radial profile of HD 142666 shows no evidence of extension (Figure 5, right panel). Combining catalogued polarization values and Hipparcos distances, Yudin et al. (1999) derived a distance-polarization law that predicts a 0.3 % contribution at V due to interstellar polarization, with a position angle of about 100 degrees at optical wavelengths. They estimated a V-band intrinsic polarization of  $p \approx 0.5$  % PA of 70 degrees. The polarization we measure in the J- band is too high to be completely interstellar in nature. In addition, we measure a polarization PA similar to that of the intrinsic op-

tical polarization estimated by Yudin et al. (1999). Yudin et al. (1999) also noted that the polarization of HD 142666 probably increases toward IR wavelengths, as is confirmed by our J- band measurements. This implies no significant interstellar contribution to the 1.2% J-band polarization that we measure, so we conclude that the polarization detected is intrinsic to the system.

#### 4.2 H- and K- band imaging polarimetry

H- and K-band imaging polarimetry was obtained for TW Hya, HD 150193 and HD 141569 on April 30th 2003. H and K photometric values are shown in Table 2, while H- and K-band polarimetric measurements are presented in Table 3. We note that HD 150193 appears fainter by  $\sim 0.4$  magnitudes in both the H- and K- band with respect to the 2MASS measurements.

TW Hya's H- and K- band imaging polarimetry are shown in Figure 6, left and right panels respectively, whilst Figure 7 shows the H- and K- band imaging polarimetry of HD 150193 (left and right panels, respectively). Alignment and subtraction residuals dominate the central parts of the images (radius $< 0.4$  arcseconds). Typical values for instrumental polarization were  $< 0.4$  percent in both H- and K-band (as measured from unpolarized standards). As in the J- band, HD 141569 did not show any evidence of extended polarized structure and is therefore not shown. The near-IR spectral dependence of the polarization for our three stars targeted at JHK is shown in Figure 8.

Figure 9, left panel, shows the JHK PI radial profiles of TW Hya. Our data show that the radial distribution of the JHK PI all follow a similar behaviour between 0.5 and 1.3 arcseconds from the star, with the polarizing disc being significantly brighter at H than it is at J and K. There is also evidence of a decrease in slope in the PI profiles from 1.3 to 2 arcseconds, as has been previously seen in direct light by Krist et al. (2000) and Weinberger et al. (2002). This reduction in slope at  $r > 1.3$  arcseconds is clear in both H and K but is less evident at J, where a bump is seen at  $r \sim 1.5$  arcseconds at very low level (see Figure 1). This is consistent with Weinberger et al.'s (2002) total intensity radial profiles, in which the change in slope is more evident at H than it is at J.

## 5 DISCUSSION

Our polarimetric imaging survey has successfully detected the presence of circumstellar polarized emission around four of our eleven targets. According to proposed CS evolutionary scenarios, both the IR excess and polarization should decrease with time (Malfait, Bogaert & Waelkens, 1998; Waelkens, Bogaert & Waters, 1994; Yudin, Clarke & Smith, 1999); as a consequence of processes such as planet formation, the discs should be cleared out and both the near-IR excess and the polarizing effects of CS dust should disappear. Thus, the detection of considerable amounts of polarizing material around TW Hya, HD 150193, HD 142666 and HD 169142 is consistent with a youthful nature. On

the other hand, the non-detection of polarized emission toward stars presenting low IR-excesses ( $L_{\text{IR}}/L_{\text{star}} < 0.1$ ) suggests that these stars are at a more advanced evolutionary state, probably near to the beginning of their MS phase. In this context we would have expected to detect polarized emission around HD 144432 and HD 143006 (which present  $L_{\text{IR}}/L_{\text{star}}$  values and near-IR excesses even higher than those of HD 142666. The most likely reasons for not detecting their discs polarimetrically could be that either we did not integrate deep enough to detect the scattered light against the stellar flux or that the disc is symmetrically distributed but unresolved, or a combination of both effects. Dominik et al. (2003) showed that the near-IR excesses of Class II sources (such as HD 144432, HD 142666 and HD 150193) can be well modelled if there is a large presence of micron-sized grains in the inner 10 AU of their CS discs. It seems reasonable to deduce that the near-IR scattering discs around HD 144432, HD 143006 and HD 142666 are too small to be resolved by UKIRT. In fact, recent VLT mid-IR interferometric observations have successfully measured the radius of HD 144432's disc to be of 0.014 arcseconds (Leinert et al., 2004), far too small to be resolved by our UKIRT observations.

Apai et al. (2004) proposed that TW Hya's disc Ks-band polarized intensity profile and the J- and H-band total intensity radial profiles have a similar behaviour, concluding that the percentage of polarization is nearly constant between 0.9 and 1.4 arcseconds from the star. As reported in Section 4.2, our observations show that in this region the JHK PI radial profiles are indeed very similar. By combining our PI radial profiles and the total intensity radial profiles from HST (Weinberger et al., 2002), we derive TW Hya's disc J- and H-band intrinsic percentage polarization as a function of radius (Figure 9, right panel). We find  $P_J$  and  $P_H$  are roughly constant between 0.9 and 1.3 arcseconds, with  $P_H$  being higher than  $P_J$  at all radii. In this region, the percentage polarization has peaks at  $27.6 \pm 6.1$  at J and  $31.3 \pm 1.5$  at H, both at a radius of 1.2 arcseconds. Beyond 1.4 arcseconds  $P_J$  falls-off, while  $P_H$  rises with increasing offset from the star. This is a consequence of the steeper J-band PI profile, as the Weinberger et al. (2002) total intensity profiles for the 1.1 and 1.6  $\mu\text{m}$  NICMOS filters have the same  $r^{-2.6 \pm 0.1}$  fitted slope. However, the NICMOS 1.6  $\mu\text{m}$  surface brightness deviates from this single power-law beyond 1.4 arcseconds, suggesting that our  $P_H$  may be overestimated beyond this radius. Nevertheless, we can conclude that our observations, in conjunction with direct light images from the HST (Weinberger et al., 2002), indicate that the disc scattering and polarizing efficiencies peak in the H-band, suggesting there is a substantial population of sub-micron sized particles present in the disc (Bohren & Huffman, 1983). This would argue against larger grains of the type suggested by Roberge, Weinberger & Malumuth (2005), although this needs to be investigated more thoroughly by future modelling.

Our imaging polarimetry for HD 169142 confirms the presence of an extended CS structure. Both the Q- and U- J-band images showed modulation with angle as was already noted by Kuhn et al. (2001), suggesting that the disc is oriented near to pole-on. The disc-size of 1.2 arcseconds we measure (174 AU at HD 169142's distance) is 0.3 arc-

seconds smaller than the previous polarized-disc extension measured by Kuhn et al. (2001). We note that the effective exposure time used by Kuhn et al. (2001) was 2.2 times larger than the one we used, which may explain the difference in HD 169142's measured disc extension between these two UKIRT observations. Kuhn et al. (2001) also detected a scattering inhomogeneity within the CS cloud, but this was not evident in our data. It is interesting to note that HD 169142 has been proposed as a Group I source (following the Meeus et al. (2001) classification) and that its SED has been successfully modelled with a flaring-disc geometry (Dominik et al., 2003) and outer disc-radius of 100 AU.

Based on the H-band disc-radius of 1.3 arcseconds measured coronographically with Subaru by Fukagawa et al. (2003), we would have expected to resolve the disc around HD 150193, at least in our H- and K-band observations. However we find no signs of extension when comparing our PI radial profiles of HD 150193 with the total intensity radial profiles of the PSF calibrator star. We believe our non-detection of the extended disc is due to sensitivity effects, since the Subaru observations carried out with a nine times longer integration time and a four times larger telescope collecting area. Even though we failed to detect the disc reported by Fukagawa et al. (2003), we believe there must still be an axisymmetric structure causing the relatively large linear polarization toward this star. The alignment of the polarization vectors at 57 degrees PA is likely to be intrinsic, and not associated with interstellar polarization (as discussed in Section 4.1). To produce the aligned vectors such structure must be (i) optically thick at J, (ii) inclined to the plane of the sky (i.e. not face on) and (iii) too small to resolve with UKIRT. So this could be an inner, optically thick component of HD 150193's disc. We also note that HD 150193 shows the steepest spectral dependence of polarization among our three JHK targeted stars, with its polarization PA being constant within the errors at all wavelengths (as can be seen in both Figure 7 and in the values presented in Tables 3). Adopting the binary PA of 225 degrees measured by Fukagawa et al. (2003), we note that there is an apparent alignment between polarization PA (57 degrees) and the axis between the two stars, although this could be just a coincidence. Nevertheless, this behaviour has already been reported in the V-band by Maheswar, Manoj & Bhatt (2002), who suggested that it is common to several other HAeBe binary systems.

We have found for HD 142666 similar evidence of a CS scattering structure to that for HD 150193. Along with HD 150193, HD 142666 exhibits a large value of linear polarization compared to the rest of our sample and also presents aligned vectors suggesting that the CS disc was unresolved. The similarity between both stars in terms of their infrared excesses and their polarization makes it plausible to suggest a similar structure in their discs. This is consistent with the SED modelling carried out by Dominik et al. (2003), in which both discs are estimated to be comparable in size and mass.

Despite the limited size of our sample, we note that our polarimetric observations detected the presence of extended polarizing discs only around systems that have had their SEDs fitted with a flared disc geometry (Calvet et al., 2002;

Dominik et al., 2003). This points toward an observational selection effect predicted by Whitney & Hartmann (1992), in which Monte Carlo scattered light models show that a flaring disc scatters up to two orders of magnitudes more light than a flat disc of similar size and mass. Detailed scattered-light modelling of our polarimetric data is, however, required to constrain the physical parameters of the detected CS discs.

## ACKNOWLEDGEMENTS

ASH carried out this work whilst being funded as part of the PPARC Gemini - Fundación Andes UK/Chile studentship programme. We thank Dr Malcolm Currie for very useful help with aspects of the data reduction. This work made use of the Starlink computing network, funded by the UK Particle Physics and Astronomy Research Council (PPARC). The UKIRT is operated by the Joint Astronomy Centre on behalf of PPARC, the Netherlands Organization for Pure Research, and the National Research Council of Canada. This work made use of the SIMBAD database and other facilities operated at CDS, Strasbourg, France, and of the 2MASS point-source catalogue available at the NASA/IPAC Infrared Science Archive, which is operated by the Jet Propulsion Laboratory, California Institute of Technology, under contract with the National Aeronautics and Space Administration. We especially thank the anonymous referee for helpful suggestions that greatly improved the article.

## REFERENCES

Apai, D., Pascucci, I., Brandner, W., Henning, Th., Lenzen, R., Potter, D.E., Lagrange, A.-M. & Rousset, G., 2004, *A&A*, 415, 671

Augereau, J. C. Lagrange, A. M. Mouillet, D. & Ménard, F., 1999, *A&A*, 350, L51

Aumann, H. H., Beichman, C. A., Gillett, F. C., de Jong, T., Houck, J. R., Low, F. J., Neugebauer, G., Walker & R. G., Wesselius, P. R., 1984, *ApJ*, 278, L23

Berry, D.S. & Gledhill, T. M., 2003, Starlink User Notes, available from <http://star-www.rl.ac.uk>

Beust, H., Lagrange, A.-M., Plazy, F., & Mouillet, D. 1996, *A&A*, 310, 181

Bohren, C. F., Huffman, D. R., 1983 "Absorption and Scattering of Light by Small Particles", Wiley, New York.

Bouwman, J., Meeus, G., de Koter, A., Hony, S., Dominik, C., Waters, L. B. F. M., 2001, *A&A*, 375, 950B

Bouvier, J., & Corporon, P., 2001, in IAU Symp. 200, The Formation of Binary Stars, ed. H. Zinnecker & R. D. Mathieu (San Francisco: ASP), 155

Calvet, N., D'Alessio, P., Hartmann, L., Wilner, D., Walsh, A. & Sitko, M., 2002, *ApJ*, 508, 1008

Crifo, F., Vidal-Madjar, A., Lallement, R., Ferlet, R. & Gerbaldi, M., 1997, *A&A*, 320, 29

Dent, W.R.F., Greaves, J.S. & Coulson, I.M., 2005, *MNRAS*, 359, 663

Dominik, C., Dullemond, C. P., Waters, L.B.F.M. & Walch, S., 2003, *A&A*, 398, 607

Dullemond, C.P. & Dominik, C., 2004, *A&A*, 417, 159

Dunkin, S.K., Barlow, M.J & Ryan, S.G., 1997a, *MNRAS*, 286, 604

Dunkin, S.K., Barlow, M.J & Ryan, S.G., 1997b, *MNRAS*, 290, 165

Fukagawa, M., Tamura, M., Itoh, Y., Hayashi, S.S. & Oasa, Y., 2003, *ApJ*, 590, L49-L52

Gledhill, T. M. Scarrott & S. M., Wolstencroft, R. D., 1991, *MNRAS*, 252, 50

Gregorio-Hetem, J., Lepine, J.R.D., Quast, G.R., Torres, C.A.O. & de La Reza, R., 1992, *AJ*, 103, 549

Krist, J.E., Stapelfeldt, K.R., Ménard, F., Padgett, D.L. & Burrows, C.J., 2000, *ApJ*, 538, 749

Kuhn, J.R., Potter, D. & Parise, B., 2001, *ApJ*, 553, L189-L191

Leinert, Ch., van Boekel, R., Waters, L. B. F. M., Chesneau, O., Malbet, F., Köhler, R., Jaffe, W., Ratzka, Th., Dutrey, A., Preibisch, Th., Graser, U., Bakker, E., Chagnon, G., Cotton, W. D., Dominik, C., Dullemond, C. P., Glazenborg-Kluttig, A. W., Glindemann, A., Henning, Th., Hofmann, K.-H., de Jong, J., Lenzen, R., Ligori, S., Lopez, B., Meisner, J., Morel, S., Paresce, F., Pel, J.-W., Percheron, I., Perrin, G., Przygodda, F., Richichi, A., Schöller, M., Schuller, P., Stecklum, B., van den Ancker, M. E., von der Lühe, O. & Weigelt, G., 2004, *A&A*, 423, 537L

Leroy, J. L., 1993, *A&AS*, 101, 551

Maheswar, G., Manoj, P. & Bhatt, H. C., 2002, *A&A*, 387, 1003

Malfait, K., Bogaert, E. & Waelkens, C., 1998, *A&A*, 331, 211

Mannings, V. & Barlow, M.J., 1998, *ApJ*, 497, 330

Meeus, G., Waelkens, C. & Malfait, K., 1998, *A&A*, 329, 131

Meeus, G., Waters, L.B.F.M., Bouwman, J., Van den Ancker, M.E., Waelkens, C. & Malfait, K., 2001, *A&A*, 365, 476

Mora, A., Merín, B., Solano, E., Montesinos, B., de Winter, D., Eiroa, C., Ferlet, R., Grady, C.A., Davies, J.K., Miranda, L.F., Oudmaijer, R.D., Palacios, J., Quirrenbach, A., Harris, A.W., Rauer, H., Cameron, A., Deeg, H.J., Garzón, F., Penny, A., Schneider, J., Tsapras, Y. & Wesselius, P. R., 2001, *A&A*, 378, 116

Natta, A., Testi, L., Neri, R., Shepherd, D. S., Wilner, D. J. 2004, *A&A*, 416, 179

Pérez, M. R., van den Ancker, M. E., de Winter, D. & Bopp, B. W., 2004 *A&A*, 416, 647

Prato, L., Ghez, A.M., Piña, R.K., Telesco, C.M., Fisher, R.S., Wizinowich, P., Lai, O., Acton, D.S. & Stomski, P., 2001, *ApJ*, 549, 590

Perryman, M.A.C., Lindegren, L., Kovalevsky, J., Hoeg, E., Bastian, U., Bernacca, P.L., Crézé, M., Donati, F., Grenon, M., van Leeuwen, F., van der Marel, H., Mignard, F., Murray, C.A., Le Poole, R.S., Schrijver, H., Turon, C., Arenou, F., Froeschlé, M. & Petersen, C.S., 1997, *A&A*, 323, 49

Roberge, A., Weinberger, A.J. & Malumuth, E.M., 2005, *ApJ*, 622, 1171

Sylvester, R.J. & Skinner, C.J., 1996, *MNRAS*, 283, 457

Sylvester, R.J., Skinner, C.J., Barlow, M.J. & Mannings, V., 1996, *MNRAS*, 279, 915

Sylvester, R.J., Skinner & C.J., Barlow, M.J., 1997, *MNRAS*, 289, 831

Sylvester, R.J., & Mannings, V., 2000, *MNRAS*, 313, 73

Vink, J.S., Drew, J.E., Harries, T.J. & Oudmaijer, René D., 2002, *MNRAS*, 337, 356

Waelkens, C., Bogaert, E. & Waters, L. B. F. M., 1994, in The Nature and Evolutionary Status of Herbig Ae/Be Stars, ed. P. S. Thé, M. R. Pérez, & P. J. van den Heuvel (San Francisco: ASP), 405

Waters, L. B. F. M.; Waelkens, C., 1998, *ARA&A*, 36, 233W

Weinberger, A.J., Becklin, E.E., Schneider, G., Chiang, E.I., Lowrance, P.J., Silverstone, M.D., Zuckerman, B., Hines, D.C. & Smith, B.A., 2002, *ApJ*, 566, 409-418

Whitney, Barbara A. & Hartmann, Lee, 1992, *ApJ*, 395, 529

Whittet, D. C. B., Martin, P. G., Hough, J. H., Rouse, M. F., Bailey, J. A. & Axon, D. J., 1992, *ApJ*, 386, 562

Yudin, R.V., Clarke, D. & Smith, R.A., 1999, *A&A*, 345, 547

Yudin, R.V., 2000, *A&A*, 144, 285

Zuckerman, B., 2001, Annual Review of Astronomy and Astro-



**Table 1.** Programme stars observed

| Name      | Sp class | $L_{\text{IR}}/L_{\star}$ | Distance [pc] | V     |
|-----------|----------|---------------------------|---------------|-------|
| HD 98800  | K5Ve     | $8.4 \cdot 10^{-2}$       | 17            | 8.86  |
| HD 123160 | G5V      | $4.4 \cdot 10^{-3}$       | 15.7          | 8.62  |
| HD 123356 | G1V      | $5 \cdot 10^{-2}$         | 41            | 9.7   |
| HD 141569 | A0Ve     | $8.4 \cdot 10^{-3}$       | 99            | 7.0   |
| HD 142666 | A8Ve     | 0.34                      | 114           | 8.65  |
| HD 143006 | G5Ve     | 0.56                      | 82            | 10.21 |
| HD 144432 | A9/F0Ve  | 0.48                      | 200           | 8.17  |
| HD 145263 | F0V      | $2 \cdot 10^{-2}$         | 116           | 8.95  |
| HD 150193 | A1V      | 0.37                      | 150           | 8.88  |
| HD 169142 | A5Ve     | $8.8 \cdot 10^{-2}$       | 145           | 8.15  |
| TW Hya    | K7 Ve    | 0.25                      | 56            | 11.1  |

Spectral classifications and IR excesses are from Sylvester et al. (1996), Dunkin, Barlow & Ryan (1997a) and Sylvester & Mannings (2000). An ‘e’ after the luminosity class indicates the presence of  $H\alpha$  emission. HD 141569, HD 123356, HD 144432, HD 150193 and HD 98800 have binary companions at separations of 6.8, 2.2, 1.2, 1.1 and 0.8 arcseconds respectively (Augereau et al., 1999; Sylvester & Mannings, 2000; Pérez et al., 2004; Mora et al., 2001; Prato et al., 2001). Distances are from the Hipparcos catalogue (Perryman et al., 1997).

**Table 2.** Photometric measurements

| name      | Filter | Magnitude       | Magnitude       | FWHM         | FWHM         |
|-----------|--------|-----------------|-----------------|--------------|--------------|
|           |        |                 | 2MASS           |              | reference    |
|           |        |                 |                 | [arcseconds] | [arcseconds] |
| HD 98800  | J      | $6.36 \pm 0.02$ | $6.39 \pm 0.02$ | 0.84         | 0.87         |
| HD 123160 | J      | $5.78 \pm 0.03$ | $5.81 \pm 0.02$ | 1.30         | 1.23         |
| HD 123356 | J      | $5.94 \pm 0.02$ | $5.89 \pm 0.02$ | 0.94         | 0.93         |
| HD 141569 | J      | $6.88 \pm 0.02$ | $6.87 \pm 0.03$ | 0.85         | 1.09         |
| HD 141569 | H      | $7.05 \pm 0.02$ | $6.86 \pm 0.02$ | 0.41         | 0.45         |
| HD 141569 | K      | $6.84 \pm 0.02$ | $6.82 \pm 0.02$ | 0.38         | 0.39         |
| HD 142666 | J      | $7.32 \pm 0.02$ | $7.35 \pm 0.02$ | 0.93         | 0.92         |
| HD 143006 | J      | $8.12 \pm 0.03$ | $8.35 \pm 0.02$ | 0.86         | 0.95         |
| HD 144432 | J      | $7.13 \pm 0.03$ | $7.09 \pm 0.02$ | 0.85         | 0.84         |
| HD 145263 | J      | $8.10 \pm 0.02$ | $8.08 \pm 0.02$ | 0.69         | 0.67         |
| HD 150193 | J      | $6.94 \pm 0.02$ | $6.94 \pm 0.02$ | 0.66         | 0.65         |
| HD 150193 | H      | $6.63 \pm 0.02$ | $6.21 \pm 0.02$ | 0.53         | 0.51         |
| HD 150193 | K      | $5.92 \pm 0.02$ | $5.47 \pm 0.02$ | 0.39         | 0.37         |
| HD 169142 | J      | $7.44 \pm 0.02$ | $7.31 \pm 0.02$ | 0.66         | 0.58         |
| TW Hya    | J      | $8.16 \pm 0.02$ | $8.21 \pm 0.02$ | 0.82         | 0.88         |
| TW Hya    | H      | $7.58 \pm 0.02$ | $7.55 \pm 0.02$ | 0.51         | 0.46         |
| TW Hya    | K      | $7.29 \pm 0.02$ | $7.29 \pm 0.02$ | 0.53         | 0.49         |

Photometry was performed using 3.5 arcsecond apertures and calibrated using observed UKIRT standards. Photometric magnitudes from the 2MASS point-source catalogue have been included. FWHMs measured both in the targeted stars and repetitive PSF references are presented.

**Table 3.** Polarimetric measurements

| name      | Filter | P [%]           | $\theta$     |
|-----------|--------|-----------------|--------------|
| HD 98800  | J      | $0.21 \pm 0.02$ | $-70 \pm 11$ |
| HD 123160 | J      | $0.12 \pm 0.01$ | $80 \pm 13$  |
| HD 123356 | J      | $0.26 \pm 0.01$ | $84 \pm 9$   |
| HD 141569 | J      | $0.55 \pm 0.02$ | $-77 \pm 9$  |
| HD 141569 | H      | $0.22 \pm 0.02$ | $-71 \pm 8$  |
| HD 141569 | K      | $0.08 \pm 0.02$ | $-59 \pm 10$ |
| HD 142666 | J      | $1.32 \pm 0.02$ | $75 \pm 3$   |
| HD 143006 | J      | $0.17 \pm 0.02$ | $6 \pm 12$   |
| HD 144432 | J      | $0.49 \pm 0.02$ | $3 \pm 8$    |
| HD 145263 | J      | $0.37 \pm 0.03$ | $23 \pm 11$  |
| HD 150193 | J      | $3.14 \pm 0.02$ | $57 \pm 4$   |
| HD 150193 | H      | $2.04 \pm 0.01$ | $52 \pm 5$   |
| HD 150193 | K      | $1.41 \pm 0.03$ | $48 \pm 6$   |
| HD 169142 | J      | $0.22 \pm 0.03$ | $-37 \pm 6$  |
| TW Hya    | J      | $0.23 \pm 0.02$ | $51 \pm 6$   |
| TW Hya    | H      | $0.18 \pm 0.02$ | $56 \pm 7$   |
| TW Hya    | K      | $0.10 \pm 0.02$ | $50 \pm 8$   |

Integrated percentage polarizations were computed using the polarimetry tool-box in GAIA<sup>†</sup>, which allows vectors within a chosen aperture to be selected for integration <sup>†</sup>(<http://www.starlink.rl.ac.uk/>). This calculates the mean Stokes Q and U values and returns the polarization integrated over the annular region defined by  $0.4 < \text{radius} < 3.5$  arcseconds. This excludes the inner regions which are usually dominated by alignment and subtraction residuals. Polarization position angles are in degrees and measured from North to East.

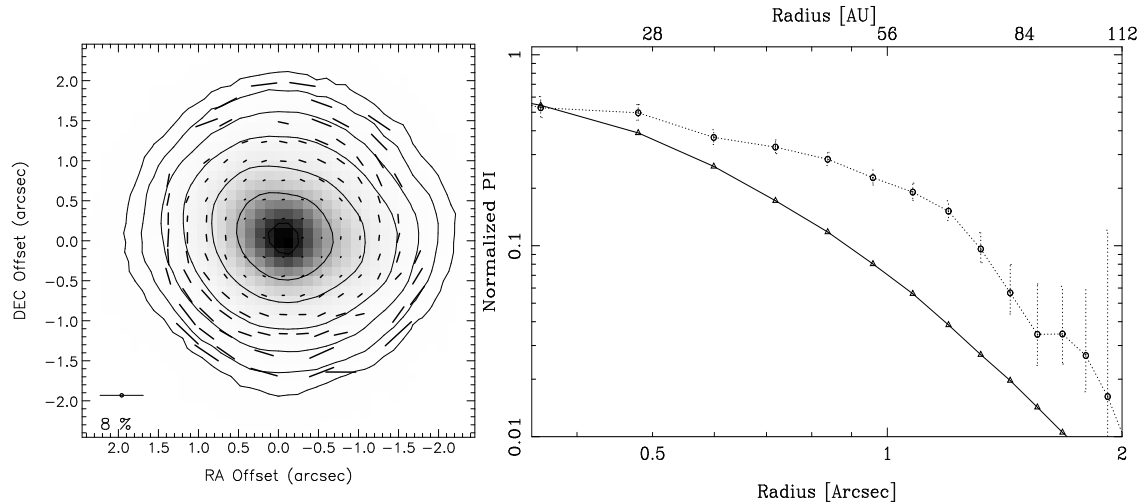


**Figure 1.** *Left panel:* J-Band imaging polarimetry of TW Hya. Polarization vector maps are superimposed upon total intensity maps, showing both contours and grey-scale images. Polarization measurements have been binned in  $3 \times 3$  square bins and a  $2\sigma$  cut applied to avoid spurious values. North is up and East is to the left. *Right panel:* Normalized radial polarized intensity distribution around TW Hya (dotted line) compared to the total intensity radial profile of the PSF calibrator star HIP 54690 (solid line). The data have been binned over 1-pixel width rings and the error bars correspond to the statistical errors of each bin. Both x- and y- axis are plotted on logarithmic scale.

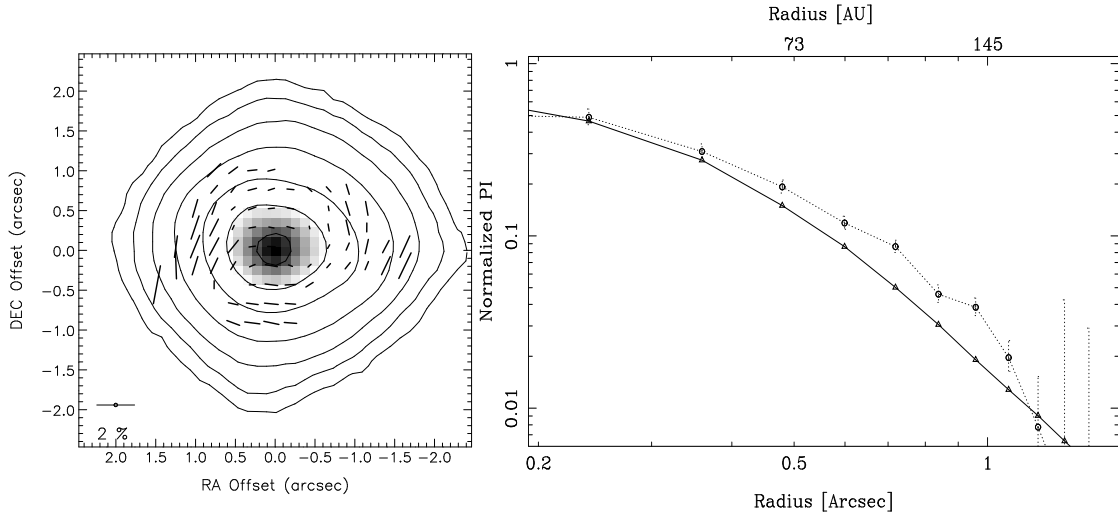


**Figure 2.** *Left panel:* J-band imaging polarimetry of HD 169142, presented in the same format as for Figure 1. The polarization vector map of HD 169142 suggests the marginal detection of a centro-symmetric pattern. *Right panel:* The J-band PI radial profile for HD 169142 (dotted line). The solid line corresponds to the total intensity radial profile of the PSF reference star, FS 140. Azimuthal values have been binned over 1-pixel width concentric rings. The error bars represent the statistical errors. Both x- and y- axis are plotted on logarithmic scale.

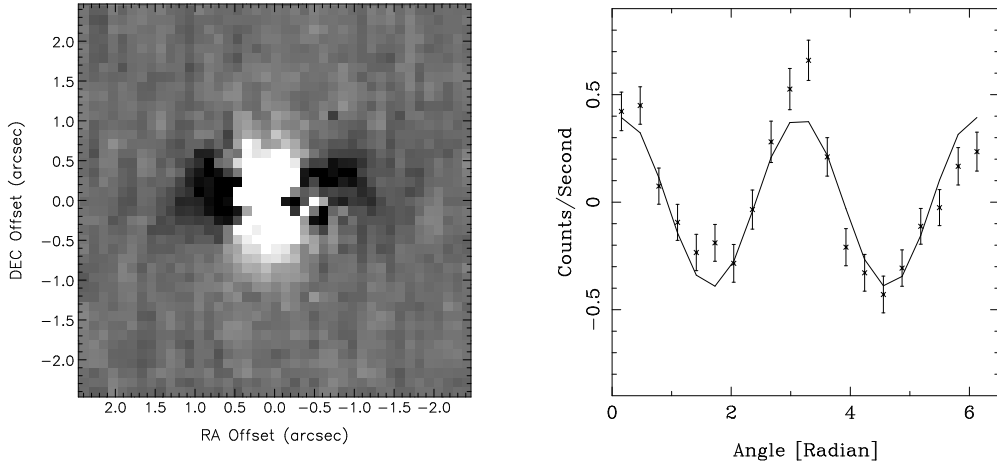


**Figure 3.** Q- Stokes image of HD 169142 (left panel). HD 169142's Q- Stokes image shows sinusoidal modulation with angle (right panel). The crosses mark the data points binned over 18 degree bins, centred on HD 169142, using an annulus extending between 0.6 and 2.2 arcseconds. The solid curve represents the best sinusoidal fit to the data.

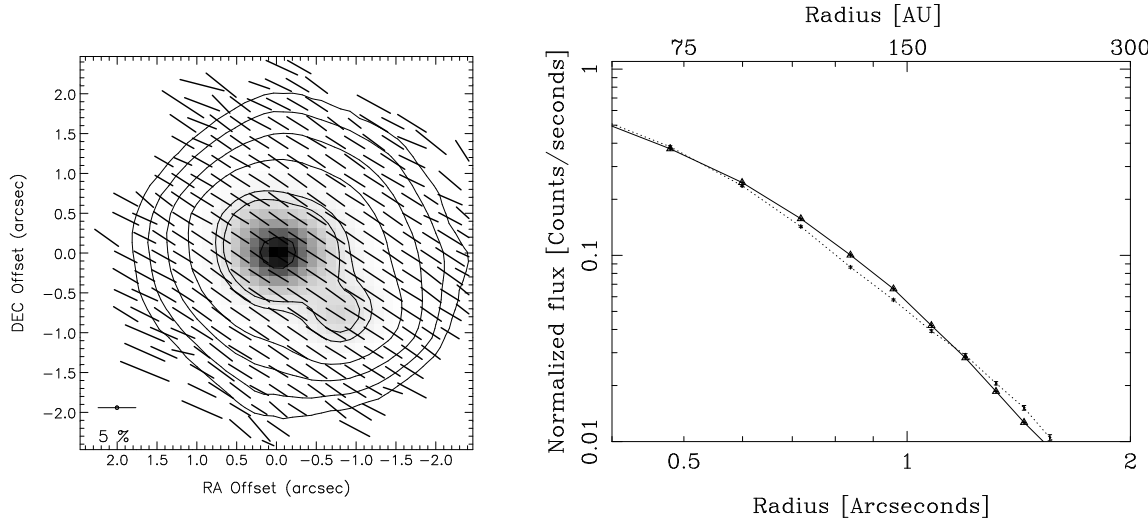


**Figure 4.** *Left panel:* J-Band imaging polarimetry of HD 150193. Polarization vectors are superimposed upon total intensity maps shown as both grey-scale and contour images. The polarization measurements have been binned in  $3 \times 3$  square bins and a  $2\sigma$  cut applied to avoid spurious values. North is up and East is to the left. *Right panel:* HD 150193 A's PI radial profile (dotted line) versus the total intensity radial profile of the PSF reference star HIP 80425 (solid line). The region containing HD 150193 B was excluded when computing HD 150193 A's PI radial profile. Both x- and y- axis are plotted on logarithmic scale.

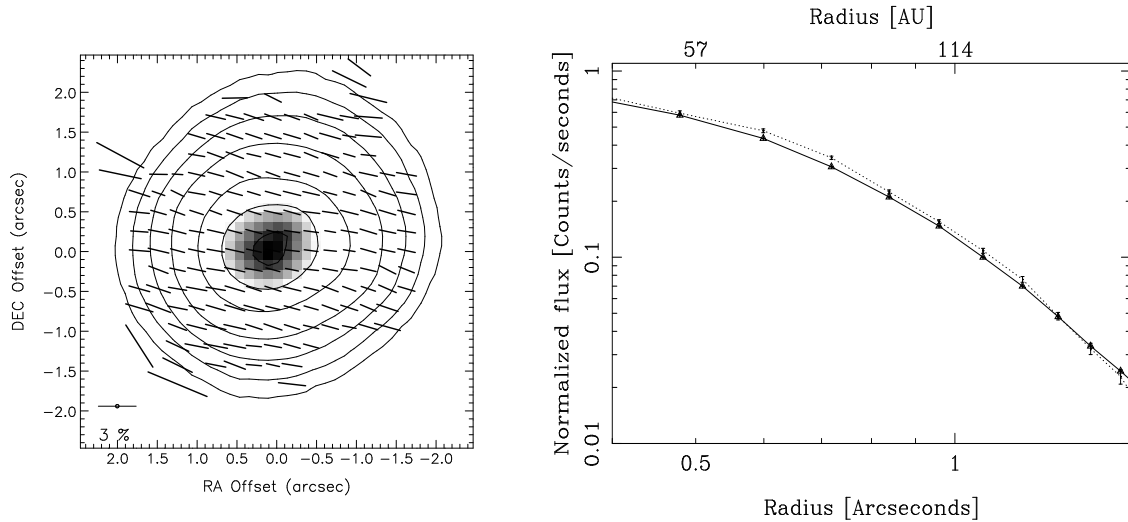


**Figure 5.** *Left panel:* J-Band imaging polarimetry of HD 142666. North is up and East is to the left. *Right panel:* HD 142666's PI radial profile (dotted line) versus the total intensity radial profile of the PSF reference star HIP 77815 (solid line). Both x- and y- axis are plotted on logarithmic scale.

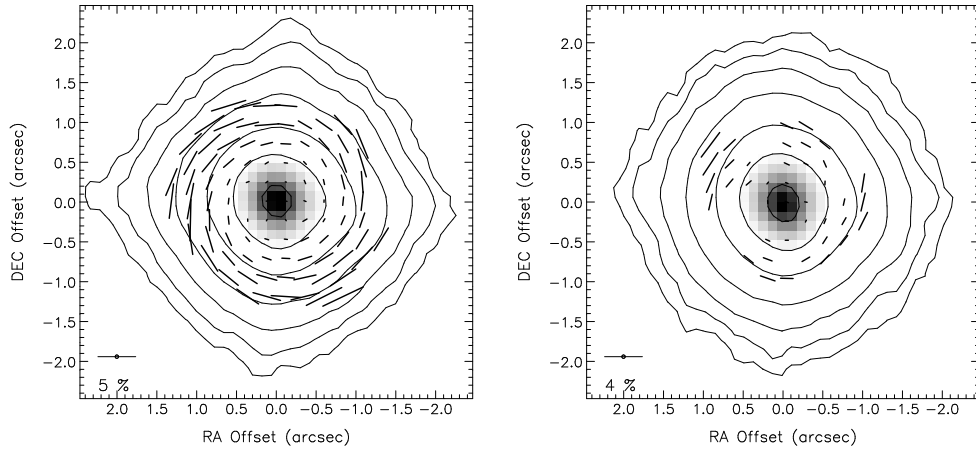


**Figure 6.** H-band (left) and K-band (right) imaging polarimetry of TW Hya. Polarization vector maps are superimposed upon total intensity maps, shown as both contour and grey-scale images. North is up and East is to the left.

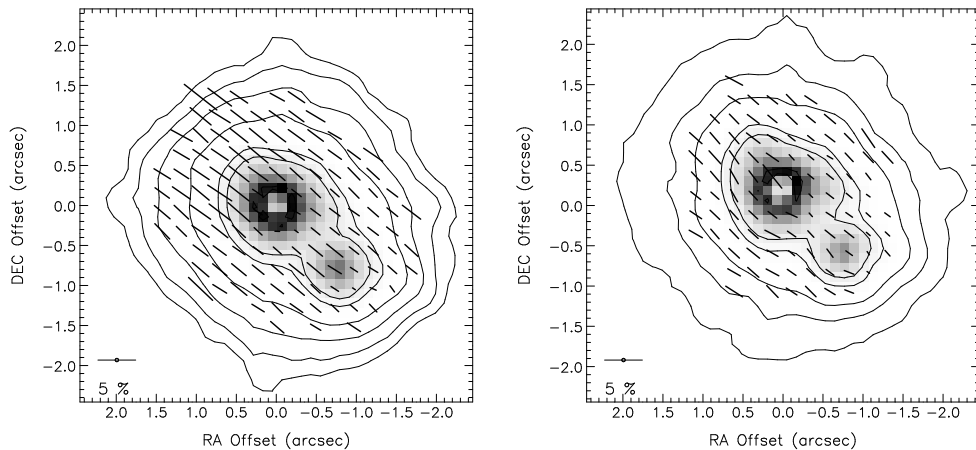


**Figure 7.** H-band (left) and K-band (right) imaging polarimetry of HD 150193. Polarization vector maps are superimposed upon total intensity contour and grey-scale images. North is up and East is to the left.

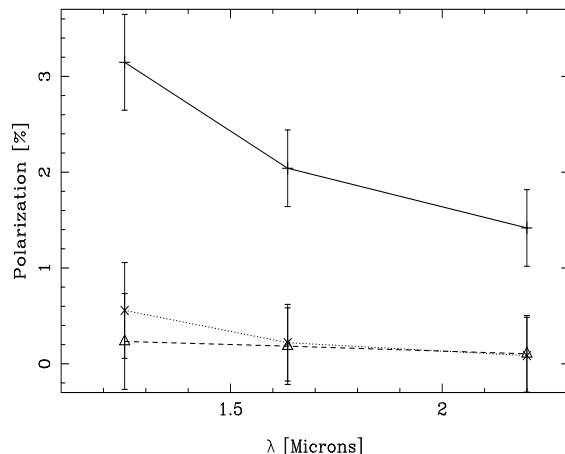


**Figure 8.** Near-IR polarization spectral dependence for HD 150193, HD 141569 and TW Hya (solid, dotted and dashed lines respectively). The error bars correspond to the instrumental errors.

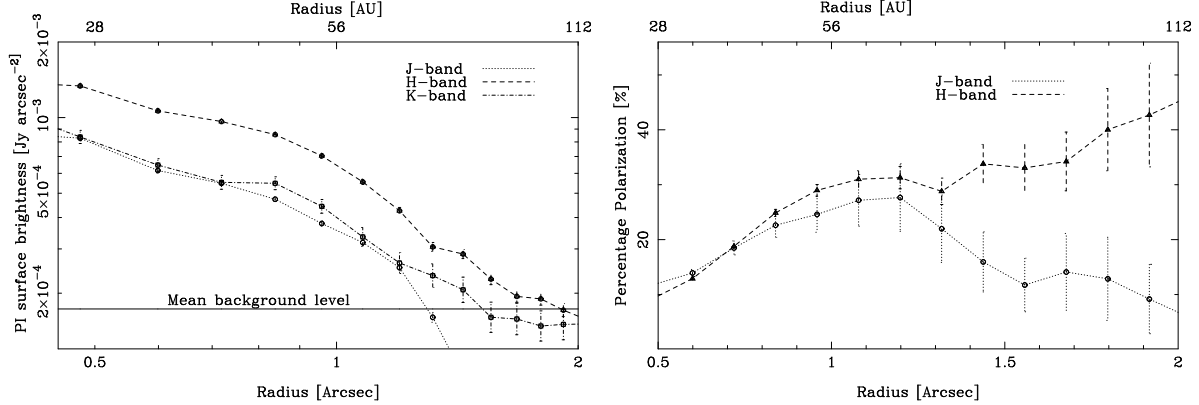


**Figure 9.** *Left panel:* J-, H- and K-band polarized intensity radial profiles of TW Hya (dotted, dashed and solid lines respectively). Both x- and y- axis are plotted on logarithmic scale. *Right panel:* J- (circles) and H-band (triangles) intrinsic percentage polarization of TW Hya's disc, derived using total intensity coronographic imaging from HST (Weinberger et al. (2002)) and our UKIRT imaging polarimetry. The error bars correspond to derived statistical errors.